Shear forces induce ICAM-1 nanoclustering on endothelial cells that impact on T-cell migration

Izabela K. Piechocka,[1,2] Sarah Keary,[1] Alberto Sosa-Costa,[1] Lukas Lau,[1] Nitin Mohan,[1,3] Jelena Stanisavljevic,[1] Kyra J. E. Borgman,[1,4] Melike Lakadamyali,[5] Carlo Manzo,[6] and Maria F. Garcia-Parajo[1,7,*]

[1]ICFO-Institut de Ciencies Fotoniques, The Barcelona Institute of Science and Technology, Barcelona, Spain; [2]Department of Biosystems and Soft Matter, Institute of Fundamental Technological Research, Polish Academy of Sciences, Warsaw, Poland; [3]Department of Biological Sciences and Bioengineering, Indian Institute of Technology, Kanpur, India; [4]Institut Curie, PSL Research University, CNRS UMR3664, Chromatin Dynamics lab, Paris, France; [5]Perelman School of Medicine, Department of Physiology, University of Pennsylvania, Philadelphia, Pennsylvania; [6]Universitat de Vic-Universitat Central de Catalunya (UVic-UCC), Vic, Spain; and [7]ICREA, Barcelona, Spain

ABSTRACT The leukocyte-specific β_2-integrin LFA-1 and its ligand ICAM-1, expressed on endothelial cells (ECs), are involved in the arrest, adhesion, and transendothelial migration of leukocytes. Although the role of mechanical forces on LFA-1 activation is well established, the impact of forces on its major ligand ICAM-1 has received less attention. Using a parallel-plate flow chamber combined with confocal and super-resolution microscopy, we show that prolonged shear flow induces global translocation of ICAM-1 on ECs upstream of flow direction. Interestingly, shear forces caused actin rearrangements and promoted actin-dependent ICAM-1 nanoclustering before LFA-1 engagement. T cells adhered to mechanically prestimulated ECs or nanoclustered ICAM-1 substrates developed a promigratory phenotype, migrated faster, and exhibited shorter-lived interactions with ECs than when adhered to non mechanically stimulated ECs or to monomeric ICAM-1 substrates. Together, our results indicate that shear forces increase ICAM-1/LFA-1 bonds because of ICAM-1 nanoclustering, strengthening adhesion and allowing cells to exert higher traction forces required for faster migration. Our data also underscore the importance of mechanical forces regulating the nanoscale organization of membrane receptors and their contribution to cell adhesion regulation.

SIGNIFICANCE Endothelial cells (ECs) form a natural barrier for regulating leukocyte migration within blood vessels. The migration of leukocytes to the places of inflammation is mediated by interactions between the integrin $\alpha_L\beta_2$ (LFA-1), expressed on leukocytes, and its ligand ICAM-1, present on activated ECs. Mechanical forces have shown to modulate LFA-1 activation, but little is known on the effect that forces have on ICAM-1. Here, we show that shear forces promote a spatial rearrangement of ICAM-1 on ECs upstream of flow and actin-dependent nanoclustering before integrin engagement. Such ICAM-1 nanoclustering impacts directly on T-cell migration by increasing T-cell velocity and shortening the interaction time with ECs. This mechanism might thus be important for firm leukocyte adhesion and migration during inflammation.

INTRODUCTION

Endothelial cells (ECs) form a natural barrier for regulating leukocyte migration within blood vessels. Leukocyte extravasation from the bloodstream to sites of inflammation or peripheral lymphoid organs involves a cascade of steps of leukocyte interactions with the activated endothelium. This multistep process includes initially low-affinity adhesive interactions (capture and rolling), firm adhesion, cell spreading and crawling, and finally, leukocyte diapedesis through the endothelial barrier to the sites of inflammation (1,2). These processes are mainly mediated by interactions between the leukocyte-specific $\alpha_L\beta_2$ integrin lymphocyte function-associated antigen (LFA-1) and its major ligand, the intracellular adhesion molecule (ICAM-1), which is highly expressed on activated ECs (3–5). The various degrees of adhesion during this cascade of events requires thus a tight regulation of LFA-1 activation and its binding strength to ICAM-1.

It is well known that LFA-1 activation is mediated by outside-in or inside-out triggering events (6–9). Avidity and lateral mobility also contribute to integrin-mediated adhesion (10,11). Moreover, tensile mechanical forces exerted by fixed ICAM-1 ligands have been recently proposed to stabilize LFA-1 in an active conformation (7,12,13). On

circulating leukocytes, lateral shear forces provided by flow conditions lead to full activation of LFA-1 through the opposing forces exerted by immobilized ICAM-1 and the actin cytoskeleton (7,14). Such force-induced changes in integrin conformation expose further ligand-binding sites, reinforcing the initially created integrin-ligand bonds and leading to increased leukocyte binding to the endothelium (15–17). However, most of these experiments have been performed on substrates containing immobilized ICAM-1 because soluble ligands are not able to activate integrins, as they do not provide the additional counterforce required to stabilize integrins in their active form (7,14,16). Intriguingly, mobility measurements of unengaged ICAM-1 showed that a large percentage of the ligand freely diffuses on the EC membrane (18). These findings are difficult to conciliate with the requirement of ICAM-1 immobilization and tensile forces to fully activate LFA-1.

Because of their localization on the EC surface, ICAM-1 molecules are continuously exposed in vivo to fluid shear stresses generated by blood flow. Together with their counter-integrin receptors, these ligand-integrin complexes therefore not only have to withstand traction forces exerted by crawling leukocytes but also have to resist forces generated by flowing blood. It has been previously shown that shear forces have an impact on ECs by inducing cell elongation along the flow direction and actin-cytoskeleton organization (19,20), focal adhesion formation (21), changes in membrane fluidity (22,23) and modulating gene regulation (24). Moreover, earlier reports showed that shear forces upregulate the expression levels of ICAM-1 (25,26). More recent work indicates that ICAM-1 is a force sensor that can initiate mechanosensitive signaling events that include actin-cytoskeleton reorganization, myosin-based contractile forces, and EC stiffness (27).

Structurally, ICAM-1 contains five extracellular glycosylated Ig-like domains, a transmembrane domain, and a short cytoplasmic tail (28). It has been also shown that ICAM-1 structurally exist as a dimer (29). Although the cytoplasmic tails contain no actin-binding motifs, clustering of ICAM-1 (induced by anti-ICAM-1 antibody (Ab)-coated beads or leukocyte binding) is capable of triggering the recruitment of cytoplasmic actin-binding proteins that anchor ICAM-1 to the actin cytoskeleton and increase its immobilization (18,27,30). Similarly, actin-regulated ICAM-1 clustering and restricted mobility have been observed on dendritic cells upon maturation (31). Yet, the lateral mobility and spatial distribution of ICAM-1 in the presence of shear force and before leukocyte engagement has not been studied in detail. It is also less known how prolonged pre-exposure of ECs to fluid shear stress affects leukocyte migratory behavior. To address these questions, we pre-exposed inflammatory challenged ECs to continuous shear flow before T-cell engagement and visualized over time the spatial distribution of ICAM-1 and the actin cytoskeleton on ECs. We show that ICAM-1 molecules are part of the shear-sensitive EC machinery that rearranges in response to continuous flow, forming nanoclusters on the EC surface that are highly localized upstream of flow. This particular spatial organization appears to be dependent on actin-cytoskeleton rearrangements induced by shear forces. ICAM-1 nanoclustering might thus contribute to strengthening interactions with integrins expressed on T cells and adhered to ECs, allowing T cells to exert larger traction forces needed for migration over the endothelium.

MATERIALS AND METHODS

Reagents, cytokines, and antibodies

RPMI-1640 Dutch modification cell culture medium without phenol red and with glutamine (2 mM) was purchased from Invitrogen (Carlsbad, CA). The medium was supplemented with 10% fetal bovine serum from Invitrogen and 1% antibiotic-antimycotic from labclinics (Barcelona, Spain). Mouse monoclonal primary Ab against ICAM-1 (anti-CD54, Cat #555510, lot 2153831, stock 0.5 mg/mL) was purchased from BD Pharmingen (San Jose, CA). Secondary Ab goat-anti-mouse-AF488 (Cat#11001, Lot# 2015565), donkey-anti-mouse Alexa 647 (Cat# A32787, Lot#UI291059), goat-anti-rabbit Alexa 647 (Cat# A21244), and donkey-anti-rabbit Alexa 647 (Cat# A32795, Lot# UG289708) were from Invitrogen. Purified ICAM-1 Fc Chimera (Cat# 721-IC, Lot# DLA1119041, stock 50 μg/mL) and mouse-anti-ICAM-1 (BBIG-I1, Cat# BBA3, Lot# ANE1319121) used for cross-linking experiments on ECs were from R&D systems (Minneapolis, MN). Polyclonal rabbit-anti-ICAM-1 (H-108, Cat# SC7891, Lot# H1712, stock 200 μg/mL) was from Santa Cruz (Dallas, TX). Phalloidin-TRITC (Cat# P-1951, Lot# 088K0459). Phalloidin-AF647 (Cat# A22287, Lot#1731699) was from Life Technologies (Carlsbad, CA) and human serum (HS) from Jackson ImmunoResearch (West Grove, PA). Tumor necrosis factor-α (TNFα), cytochalasin D (CytoD), saponin, phosphate-buffered saline (PBS), bovine serum albumin, and paraformaldehyde were from Sigma-Aldrich (St. Louis, MO). Goat-anti-mouse Ab conjugated to Cy3B was prepared in house.

Cell culture and sample preparation

We used an EC line, EA.hy926, established elsewhere by fusing primary human umbilical vein cells with a thioguanine-resistant clone of A549 by exposure to polyethylene glycol. ECs and Jurkat T lymphoblastoid (a T-cell model) were a gift from Alessandra Cambi (Nijmegen, the Netherlands). For all the experiments shown here, ECs were plated on coverslips functionalized with fibronectin (20 μg mL^{-1}) and grown to near confluency in RPMI-1640 medium at 37°C humidified atmosphere and in the presence of 5% CO$_2$. We chose near rather than full confluency because EC elongation along the flow in an in vitro setting is either observed on fully confluent cells after prolonged shear-flow stimulation (typically 24 h) or at shorter times when seeding the cells slightly below full confluency (19,20,32,33). We opted for the latter to reduce the experimental times and minimize the occurrence of bubbles inside the chamber. To mimic inflammatory conditions, samples were activated with TNFα (10 ng mL^{-1}) for 20 h before experiments. In experiments with T cells, cells were collected by centrifugation at 1200 rpm and resuspended to a concentration of 3×10^6 mL^{-1} in RPMI-1640 medium. In experiments with the actin-disrupting agent, a mild concentration of cytoD (5 μg mL^{-1}) was flown over 4 h shear-flow TNFα-stimulated ECs and left in the absence of flow for 20 min. This amount of CytoD and the time of treatment (20 min) were sufficient to perturb the actin cytoskeleton while maintaining overall EC morphology unaltered.

Microfluidics

Shear flow experiments were performed with a parallel-plate closed flow chamber (FCS2; Bioptechs, Butler, PA) that provides laminar flow. A

40 mm coverslip with a preformed EC monolayer was placed on the micro-aqueduct slide separated by 100-μm-thick gasket with a rectangular surface (1.4 × 2.2 cm). The fully assembled flow chamber was mounted on the stage of an inverted microscope (Olympus IX71; Tokyo, Japan) equipped with 20×/0.5 NA air objective and a video camera (CMOS; Thorlabs, Newton, NJ). A 37°C controlled temperature enclosure surrounding the microscope was used to maintain a constant temperature across the microfluidics. The flow chamber was connected on one end to an automated syringe pump (FCS2 Micro-Perfusion Pump) and on the other end to a medium reservoir. 5% CO_2-enriched RPMI-1640 cell culture medium of 37°C was perfused at a constant shear flow of 8 dyn cm^{-2} through the chamber. The shear stress of flowing medium τ, was calculated using the equation $\tau = (6Q\mu)/(wh^2)$, where Q is the flow rate, μ is the viscosity of the fluid, w is the width, and h is the height of gasket.

T-cell adhesion under flow

TNFα-stimulated ECs were exposed to 4 h of continuous, laminar shear flow at 8 dyn cm^{-2} before T-cell adhesion. Next, a suspension of T cells was flown over ECs using RPMI-1640 perfusion medium at 0.3 dyn cm^{-2}. Because nonactivated T cells cannot be captured directly from the flow stream, the flow was stopped to allow T cells to settle freely on ECs for 3 min. Then, the flow was resumed at 1 dyn cm^{-2} (postflow). T-cell movement was recorded for 20 min by differential interference contrast microscopy (DIC) at three frames/s^{-1} using a 10×/0.25 NA air objective. In static experiments, T cells were flown over ECs that were not subjected to shear flow beforehand. Additionally, as control, T cells were flown over static or shear-flow prestimulated ECs, without postflow application. In these cases, T cells migrated randomly.

Preparation and single-molecule characterization of monomeric and nanoclustered ICAM-1 substrates

ICAM-1 nanoclusters were prepared following a protocol as reported by (34). Briefly, purified ICAM-1-Fc was mixed with polyclonal antibodies in 1% HS at a final volume of 135 μL (final concentrations of 19 and 20 μg mL^{-1}, respectively) and placed in an incubator at 37°C for 1 h. ICAM-1 substrates were then prepared in sterile glass-bottom petri dishes. Fully covered substrates of nanoclustered ICAM-1 were produced by covering the glass-bottom petri dish with 120 μL of the previously prepared aggregated solution. Fully covered substrates of monomeric ICAM-1 were produced by covering the glass-bottom petri dish with 120 μL of 19 μg mL^{-1} purified ICAM-1 Fc. Full substrate coverage was confirmed by fluorescence inspection. Notice that the overall ICAM-1 density on both type of substrates (monomeric versus nanoclustered ICAM-1) was kept similar to allow for a robust comparison on the effect of ICAM-1 nanoclustering. Additional monomeric ICAM-1 substrates at varying ICAM-1 densities were also prepared for control experiments.

To assess the formation of ICAM-1 nanoclusters, we prepared substrates using the same solutions as mentioned earlier (either monomeric or nanoclustered) but at much lower concentration (0.475 μg mL^{-1}) to allow for characterization at the single-molecule level. Characterization of the samples was performed using the Nikon TIRF setup (Tokyo, Japan) by imaging with a 647 nm laser at 20%, 20 ms exposure time, and a pixel size of 160 nm. For this, the low-density monomeric sample was incubated with primary mouse-anti-ICAM-1 at 5 μg mL^{-1} for 45 min. The low-density nanocluster samples did not require extra primary antibodies because the secondary antibody was already tagged to the primary antibody used to make the nanoclusters. The samples were washed using PBS, and secondary antibodies were used. Donkey-anti-mouse Alexa 647 targeted the anti-ICAM-1 on the monomeric samples, and donkey-anti-rabbit Alexa 647 targeted the polyclonal anti-ICAM-1 for the nanoclusters.

T-cell adhesion and migration on ICAM-1 substrates

Fully covered ICAM-1 substrates were washed with sterile PBS and then covered with cell media. T cells were added, and the samples were placed in the microscope incubation chamber for 10 min for cells to settle. 20 min videos were then taken at 37°C and 5% CO_2 using a 10× air objective at a frame rate of three frames/s^{-1}. After each 20 min video, the objective was changed for a 20× objective, and cells were imaged for a further 10 min with the same frame rate. These 10 min videos were then used for the phenotype classification experiments.

Preparation of ECs with antibody-cross-linked ICAM-1 and T-cell adhesion

TNFα-stimulated monolayers of ECs were prepared as indicated earlier. To artificially generate ICAM-1 clusters on ECs we followed a protocol close to the one described by (35). In brief, after stimulation with TNFα, ECs were washed gently with sterile PBS, covered with 1 μg mL^{-1} of monoclonal ICAM-1 antibody diluted in cell media, and returned to the incubator for 45 min at 37°C. ECs were again washed twice with PBS, and the secondary antibody to cross-link ICAM-1 (1 μg mL^{-1}) was added for 20 min at 37°C. T cells were then added to the TNFα-stimulated and ICAM-1 cross-linked ECs monolayers and allowed to settle for 5–10 min. The T-cell movement was recorded for 20 min at three frames/s^{-1}, using a 10× air objective.

Immunofluorescence labeling

Resting (without TNFα stimulation), TNFα-stimulated, static (without mechanical prestimulation), and/or shear-flow-exposed ECs were washed with warm PBS, fixed in ambient conditions with 2% paraformaldehyde for 15 min, and immediately stained. Samples were incubated with blocking agents (3% bovine serum albumin, 10 mM glycine, and 1% HS) for 30 min and washed. Next, cells were incubated with primary antibodies against ICAM-1 (5 μg mL^{-1}), washed, and incubated further with the appropriate secondary antibody (2 μg mL^{-1}) for 30 min. In all cases, cells were stained simultaneously for F-actin with phalloidin-TRITC (0.25 μg mL^{-1}) for 40 min, after initial permeabilization of the cell membrane with saponin (0.05%) for 10 min. Static ECs were double stained for ICAM-1 and F-actin and used as a control. All individual labeling steps were carried out at room temperature. Samples for stochastic optical reconstruction microscopy (STORM) imaging were immunostained as described earlier using phalloidin-AF647 for labeling the actin cytoskeleton and antibody-conjugated Cy3B for ICAM-1 staining after initial permeabilization of the cell membrane with Triton (0.002%) for 8 min.

Confocal microscopy

Fluorescence images of ECs were acquired using a laser-scanning confocal microscope (Eclipse TE2000; Nikon). Samples were excited at 488 and 561 nm to visualize ICAM-1 and F-actin, respectively. Cross talk between detection channels was avoided by the use of appropriate excitation and emission bandpass filters. In addition, fluorescence images of ICAM-1 and F-actin were recorded separately by performing a sequential scanning and merged afterward. Three-dimensional image stacks were obtained by scanning through the z-direction in steps of 0.1 μm over a range of 20 μm using a piezo-driven 60×/1.49 NA oil immersion objective.

Stimulated emission depletion microscopy

Super-resolution images of ICAM-1 expressed on ECs were collected using a commercial continuous wave-stimulated emission depletion (STED)

microscope (Leica Microsystems Wetzlar, Germany) using 100×/1.4 NA oil immersion objective. Samples were excited with an argon-ion laser (488 nm). Images (1024 × 1024 pixels) were acquired with 12-bit pixel depth, recorded in resonant scan mode at speed of 8 kHz, and averaged over eight frames with line accumulation set at 8. The STED spatial resolution was ∼90 nm as estimated from the size of isolated spots localized at the glass substrate that represent single fluorescence antibodies.

Dual-color STORM

Super-resolution images of the actin cytoskeleton and ICAM-1 were acquired with a custom-made STORM microscope setup using a standard imaging buffer (1 M Cysteamine MEA, 0.5 mg mL^{-1} glucose, 5% glucose oxidase, and 40 μg mL^{-1} catalase in PBS; mixed at a volume ratio of 80:10:10:1). Samples were excited at 647 nm (actin) and 560 nm (ICAM-1), and reactivation of dyes was done with a laser beam at 405 nm. The emitted light was collected with 100×/1.49 NA oil immersion objective, filtered by a quad band filter set (TRF89902-ET-405/488/561/647 Laser Quad Band Set; Chroma Technology Corp, Bellows Falls, VT) and imaged with an electron-multiplying CCD camera at an exposure time of 20 ms per frame. Images were analyzed using custom-written software (Insight3; provided by Bo Huang, University of California, San Francisco, CA) by fitting the point spread function of individual fluorophores with a simple Gaussian curve in every frame to determine the x and y coordinates. The STORM spatial resolution was ∼25 nm as estimated by calculating the closest resolved distance between two neighboring microtubules stained with Alexa 647 in BSC1-African green monkey kidney epithelial cells in separate control experiments.

Image analysis

Quantification of ICAM-1 and actin fluorescent intensity from confocal images

The total fluorescence intensity signal of ICAM-1 was calculated as an integrated density signal extracted from individually outlined ECs using the ImageJ software. The z-projected intensity of 80 frames over 8 μm distance, normalized to the cell surface area, is reported. The percentage of the total ICAM-1 fluorescence intensity signal localized either up- or downstream of flow was estimated from 50% of the desired cell area and divided by the total intensity calculated over the entire cell. The fluorescent intensity of ICAM-1 localized within patch-like actin structures at the apical cell membrane was calculated by manually outlining the desire actin regions and integrating the corresponding ICAM-1 density signal over the selected areas.

Quantification of ICAM-1 nanoclustering from STED images

Unprocessed, super-resolution STED images were analyzed using custom-written MATLAB (The MathWorks, Natick, MA) software. The analysis is based on a two-dimensional Gaussian fit to the intensity profile of manually selected spots from the images. The fitting procedure determines the spot size taking a full width at half maximum of the Gaussian fit. The spot intensity (brightness) is calculated as the average of the background-subtracted intensity values over all pixels located within the full width at half maximum. To estimate the degree of nanoclustering, the brightness of the spots on the cell membrane were directly compared with that of individual Abs sparsely located on the glass coverslip, outside the cell regions.

Quantification of the number of T cells adhered to ECs after postflow application

Phase contrast images of 0.05 μm^2 were taken before and after postflow application, and the number of adherent T cells in the field of view was counted manually.

Generation of T-cell trajectories and T-cell morphology quantification

The interaction of individual T cells with ECs were followed frame by frame from DIC images using a custom-written MATLAB software. A cross-correlation function was used to estimate changes in the centroid position of individual T cells over time as described elsewhere (36). Centroid positions were then joined together to generate individual T-cell trajectories. In addition, T cells were classified based on cell shape morphology as "round" (circular morphology), "comet-like" (circular morphology but with a visible protrusion at the back of the migrating cell), and "amoeba-like" (spread morphology in various orientations).

Analysis of T-cell trajectories on ECs

A bottom-up type of algorithm for reconstruction and segmentation of noisy time traces was used to evaluate changes in the velocity and time of interaction of T cells with ECs (37). In brief, the algorithm segments the distance versus time trajectories using a piecewise linear approximation that detects changes in the slope of the trajectory and allows the reconstruction of time-trace data as consecutive straight segments. For each segment, we then extract its velocity (i.e., instantaneous velocity) and its temporal duration (i.e., interaction time). The instantaneous cell velocity at each time segment was calculated as the square root of a sum of velocities analyzed in the direction perpendicular (V_x) and parallel (V_y) to the flow. Positive (V_+) and negative (V_-) signs were assigned to each instantaneous velocity value to distinguish between periods where T cells move along or against the direction of flow, respectively. Accordingly, the positive (t_+) and negative (t_-) times of T-cell interactions with ECs were obtained. Cumulative frequency distributions of the instantaneous positive and negative velocities (and interaction times) were generated per individual experiment (containing multiple cells) and the mean value of each cumulative frequency distribution was then extracted. Data plotted in Fig. 6, C–F, correspond to the mean ± SD across different N.

Analysis of T-cell migration on ICAM-1 substrates and on ICAM-1 cross-linked ECs

The videos taken on a 10× air objective were analyzed first in Fiji and then in Python3 in the following way: first, the Fiji edge detection was used for contrast improvement. A TrackMate plugin was used for generating single tracks of the cell movement. Trajectories were then exported to Fiji/Python3 for calculating the instantaneous velocity between consecutive frames. For quantifying the cell phenotype, the videos taken on a 20× air objective were used to have increased resolution. The phenotypes were counted manually by eye using the Cell Counter plugin in Fiji (ImageJ).

Statistical analysis

Data are expressed as mean ± standard deviation (SD). The statistical significance between the means was analyzed using GraphPad Prism 6. The unpaired two-tailed Student's t-test was used to determine the statistical differences between two individual data sets. A one-way analysis of variance test, followed by the Tukey's multiple comparison test, was used to compare three or more data sets. The p-values are indicated.

RESULTS

Prolonged shear stress induces global translocation of ICAM-1 upstream of flow regardless of inflammatory EC activation

To decouple the effect of mechanical forces from biochemical stimulation of ECs, we first investigated the effect of shear stress on ICAM-1 expression and distribution on ECs, i.e., without biochemical stimulation, at the single-cell level. We

A

B

C
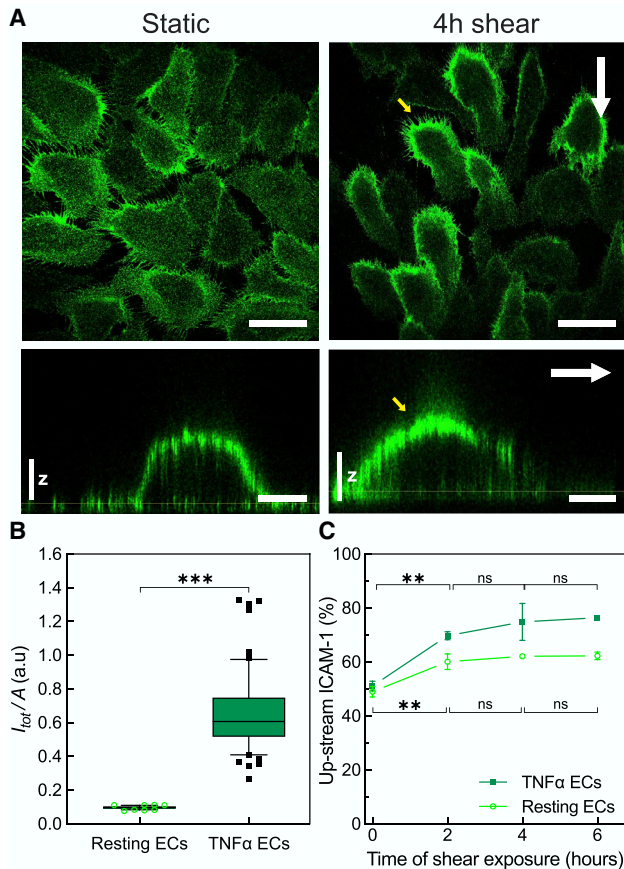
FIGURE 1 Shear flow induces global translocation of ICAM-1 upstream of flow regardless of inflammatory EC activation. (*A*) Representative single-plane confocal microscopy images taken at the basal cell membrane (*top rows*) and three-dimensional orthogonal views (*bottom rows*) of ICAM-1 expressed on TNFα-stimulated ECs in the absence (*left*) and presence of 4 h continuous shear flow (*right*). White arrows indicate the direction of flow. Yellow arrows point at the upstream accumulation of ICAM-1 upon shear-force application. Scale bars, 50 μm in top images and 15 μm in bottom images. Vertical scale z, 3 μm. (*B*) Fluorescence intensity of the ICAM-1 signal integrated over the entire cell and normalized to the cell area for resting and for TNFα-stimulated ECs in static conditions, i.e., without flow application. Bars show the median fluorescence intensity (quartile distribution in boxes; 10–90 percentile in whiskers, individual symbols are outliers) corresponding to $n = 40$ cells (resting) and $n = 60$ cells (TNFα) for one representative experiment. Significance calculated within the experiment shown (a total of $N = 3$ and $N = 5$ independent experiments for resting and TNFα, respectively, were performed). (*C*) Percentage of upstream ICAM-1 fluorescence signal taken from individual ECs under resting (*open symbols*) and TNFα-stimulated (*closed symbols*) conditions as a function of shear-force application. The signal was estimated from 50% of the desired cell area and divided by the total intensity calculated over the entire cell. Data correspond to mean $\pm$ SD over $N = 3$ independent experiments per condition (resting and TNFα-treated ECs) and shear-time exposure, with more than $n = 100$ cells per shear-time exposure and per condition. The lack of error bars in some of the data points in (*C*) is due to the small SD values as compared with the size of the symbol. Significance calculated across N. ***$p < 0.001$; **$p = 0.01$; ns, not significant. To see this figure in color, go online.

exposed resting ECs to a continuous shear flow of 8 dyn cm^{-2}, fixed the cells at different time points after different times of shear flow stimulation, labeled ICAM-1, and visualized its

overall distribution on individual cells by confocal microscopy (Fig. S1 *A*). In static conditions, ICAM-1 was barely detectable and uniformly distributed through the entire cell body (Fig. S1 *A*). Application of shear stress resulted in a twofold increase of the ICAM-1 signal over the course of 6 h (Fig. S1 *B*). These results are consistent with earlier flow cytometry studies showing that shear forces are capable on their own of upregulating ICAM-1 levels on ECs (25,26).

To test the effect of prolonged shear flow exposure on the expression levels and spatial distribution of ICAM-1 in the presence of inflammatory conditions, we treated ECs with TNFα, an inflammatory cytokine known to upregulate ICAM-1 expression. As expected, TNFα treatment resulted in translocation of ICAM-1 to the cell membrane, mostly to the apical side (Fig. 1 *A* and *z*-projections), and its de novo expression, with a sixfold increase in the total ICAM-1 intensity as compared with resting ECs (Fig. 1 *B*).

Interestingly, shear flow induced a strong gradient on ICAM-1 distribution on the apical cell membrane, with the highest ICAM-1 levels upstream of flow, i.e., the direction from which flow is initiated (Fig. 1 *A*, *yellow arrows*). This upstream accumulation was dependent on flow exposure time, being already significant at 2 h and reaching a plateau after 4 h of shear stimulation (Fig. 1 *C*). A similar trend was also observed on resting ECs (i.e., without TNFα stimulation) (Fig. 1 *C*, *open symbols*) indicating that ICAM-1 relocation upstream of flow was solely due to shear-force stimulation. Together, these data show a synergistic effect of biochemical and mechanical stimulation on the expression and spatial distribution of ICAM-1 on ECs. Whereas TNFα upregulates ICAM-1 expression and induces translocation to the apical membrane, shear stress leads to a pronounced gradient in ICAM-1 apical redistribution, with the highest levels located upstream of flow.

Prolonged shear stress induces differential actin-cytoskeleton rearrangements upstream and downstream of flow

It has been extensively documented that application of shear stress induces elongation and formation of actin fibers aligned to the flow direction (19). Confocal images of the actin cytoskeleton on ECs in the absence and after 4 h of shear flow stimulation confirmed cell elongation and actin-cytoskeleton rearrangements (Fig. 2 *A*; Fig. S2, *A–C*). Moreover, most of the actin fibers aligned along the flow direction but were preferentially located downstream of the flow, i.e., away from the flow (Fig. 2 *A*, enlarged images). In contrast, a finer actin mesh, difficult to resolve by diffraction-limited confocal microscopy, appeared upstream of the flow direction (Fig. 2 *A*). To gain more information on these finer actin structures, we performed super-resolution imaging by means of STORM (Fig. 2 *B*). With an effective increased resolution of ~25 nm, we clearly resolved the formation of actin patches located preferentially upstream of the flow direction after 4 h
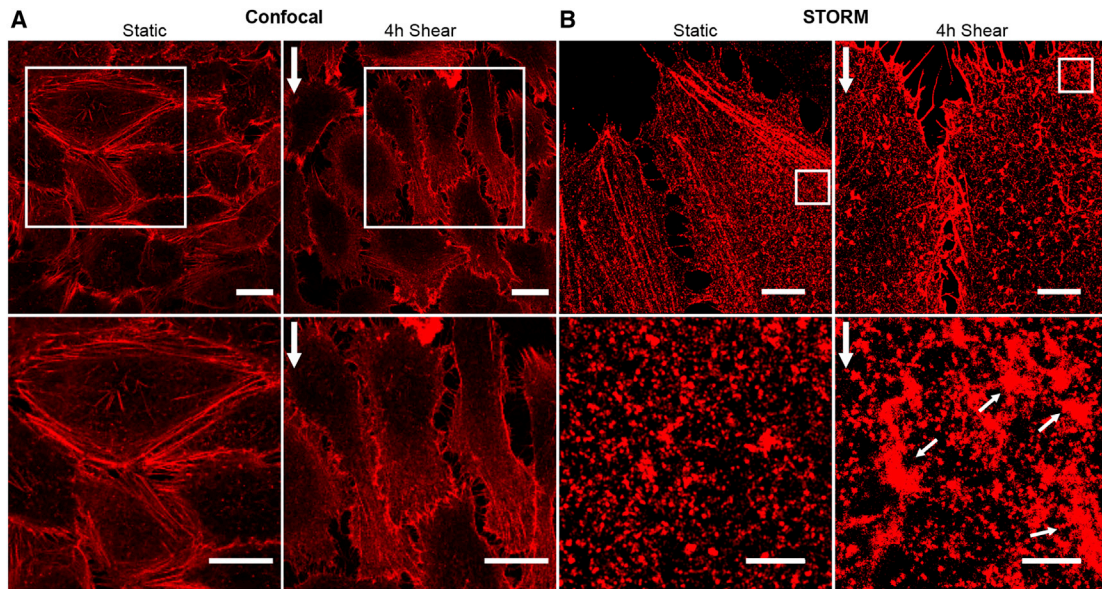
FIGURE 2 Prolonged shear stress induces differential actin-cytoskeleton rearrangements upstream and downstream of flow. (*A*) Representative *z*-projection confocal microscopy images (*top*) and magnified images (*bottom*) of the actin cytoskeleton on TNFα-stimulated ECs in the absence (*left*) and presence of 4 h continuous shear flow (*right*). Vertical white arrows on the right indicate the flow direction. Scale bars, 20 μm. (*B*) Representative STORM images (*top*) and corresponding magnified images (*bottom*) of the actin cytoskeleton in static TNFα-treated ECs (*left*) and after 4 h of shear-flow exposure (*right*). Vertical white arrows indicate the direction of the flow. Small white arrows point to actin patch-like structures. Scale bars, 5 μm (*full images*) and 1 μm (*zoom regions*). To see this figure in color, go online.

of shear-flow exposure (Fig. 2 *B*, *small white arrows*). The area occupied by these actin patches were between 1 and 5 μm^2, which is at least twofold larger than any small actin puncta observed in static ECs (Figs. 2 *B* and S2 *D*). Interestingly, the location of these actin patches coincided with regions of high ICAM-1 accumulation, prompting us to investigate the potential spatial relationship between them by confocal and super-resolution STORM.

Patch-like actin structures localize with ICAM-1-rich regions upstream of flow

We first used dual-color confocal microscopy to investigate the spatial correlation of actin and ICAM-1 in cell regions upstream of flow direction. We identified highly dense regions of actin patches together with ICAM-1 after 4 h of shear-flow stimulation, as compared with the more discrete puncta detected in static conditions (Fig. 3 *A*). Image quantification showed more than a twofold increase in the surface area occupied by these patch-like actin structures (Fig. 3 *B*), and the intensity of ICAM-1 concomitantly increased in these regions as compared with static conditions (Fig. 3 *C*). These changes were accompanied by an increase in the overall colocalization between both structures (Pearson coefficient 0.47 vs. 0.34, for shear-flow and static conditions, respectively; Fig. S2 *E*).

To gain more insight into the nanoscale rearrangement of both actin and ICAM-1, we applied dual-color STORM. Because this technique works best under total internal reflec-

tion illumination, we restricted our imaging to cortical regions located just above the basal cell membrane and upstream of flow. Concomitant to the reorganization of the actin cytoskeleton, we observed numerous discrete ICAM-1 spots, indicative of ICAM-1 nanoclustering (Fig. 3 *D*). Moreover, a large majority of the ICAM-1 spots appear to reside inside or in close proximity to the shear-induced actin patches (Fig. 3 *D*, *white outlines*). To quantify these results, we generated masks of the STORM actin signal, superimposed to them the single-molecule localizations events obtained from the ICAM-1 channel, and calculated the percentage of localizations falling into the actin mask (Fig. S3). The results confirm a significant increase of ICAM-1 colocalization with actin patches after application of flow, as compared with nonstimulated cells (Fig. 3 *E*). The results were further validated by in silico simulations of randomly distributed ICAM-1 localizations (using the experimentally obtained ICAM-1 densities in each condition) with respect to the experimentally generated actin mask (Fig. 3 *E*). Overall, these data reveal a clear shear-flow-induced actin reorganization upstream of flow direction that is accompanied by selective ICAM-1 recruitment to these dense actin regions.

Shear flow induces the formation of actin-dependent ICAM-1 nanoclusters on TNFα-stimulated ECs

Our STORM data showed the presence of discrete ICAM-1 spots on the cell membrane, suggesting the formation of
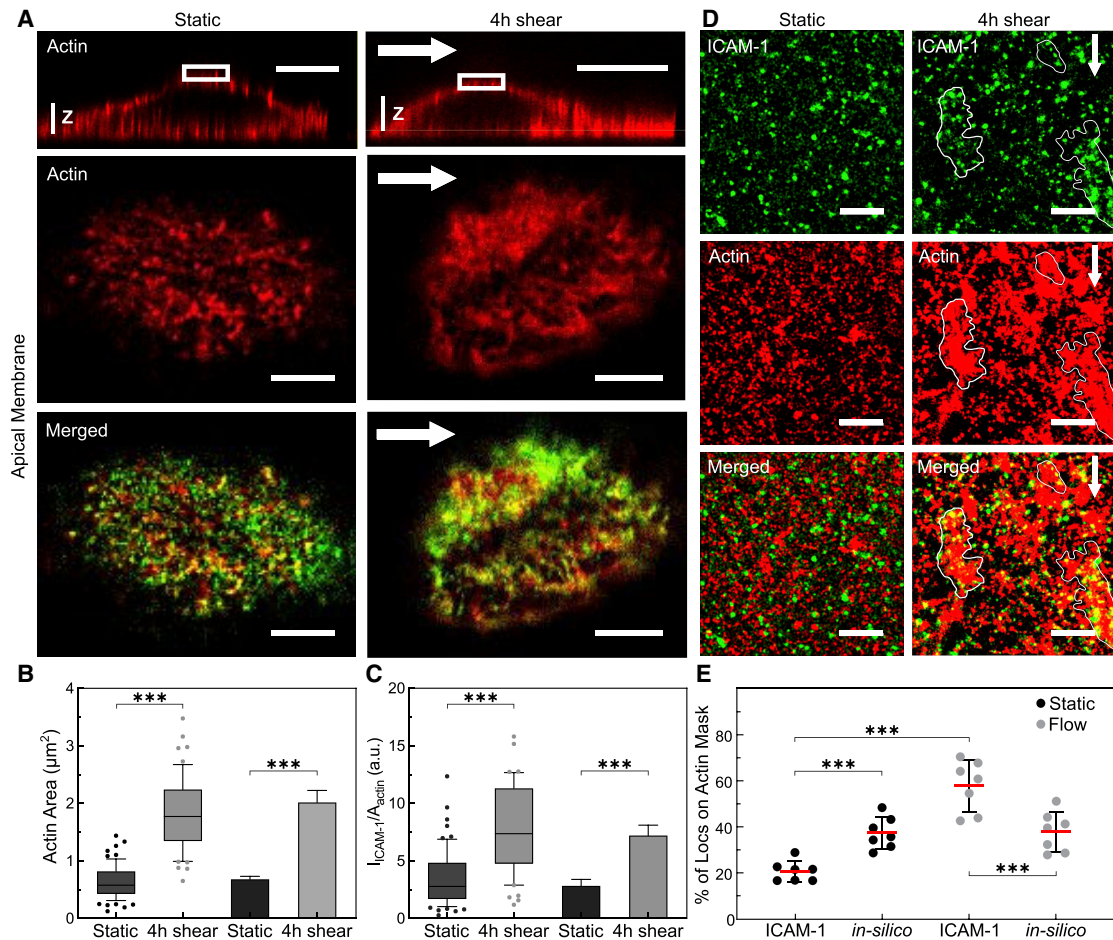
FIGURE 3 Shear flow promotes the formation of patch-like actin structures that localize with ICAM-1 rich regions upstream of flow. (A) Three-dimensional orthogonal views (*top row*) and magnified single-plane confocal microscopy images (*middle* and *bottom rows*) of the cortical actin cytoskeleton (*red*) and ICAM-1 (*green*) localized at the apical cell membrane in static (*left*) and 4 h shear-flow TNFα-stimulated ECs (*right*). White arrows indicate the direction of flow. Scale bars, 20 μm (*top images*) and 5 μm (*bottom images*), respectively. Vertical scale *z*, 3 μm. (B) Area occupied by puncta-like or patch-like actin structures, calculated from manually outlining actin regions on static ECs or 4 h sheared ECs. (C) ICAM-1 fluorescent intensity in regions enriched by actin puncta or patches, normalized to their corresponding actin area, for static and 4 h sheared ECs. Box and whiskers plots in (B) and (C) (*lines* show median values, quartile distribution in *boxes*; 10–90 percentile in *whiskers*, individual symbols are outliers) show data for one representative experiment per condition, with significance calculated within the experiment. 6–10 actin structures (puncta-like or isolated patches) per cell, $n = 10$ cells for static and $n = 8$ cells for 4 h shear. Bar plots in (B and C) correspond to the mean $\pm$ SD for N = 5 and N = 3 independent experiments for static and 4 h sheared ECs, respectively, with significance calculated across N. (D) Dual-color STORM images on TNFα-stimulated ECs of ICAM-1 (*top*), actin (*middle*), and merged images (*bottom*) located upstream of the cells, in the absence (*left*) and after 4 h shear-flow (*right*). White arrows show the direction of applied shear flow. White contours highlight regions where ICAM-1 colocalizes with patch-like actin structures. Scale bar, 1 μm. (E) Percentage of ICAM-1 single-molecule localizations residing inside the actin mask areas for static and 4 h shear-flow stimulated ECs. Symbols correspond to the calculated percentage per individual region of interest analyzed. In silico data correspond to similar analysis but performed by randomly distributing the total number of ICAM-1 localizations obtained from each corresponding experimental condition on the corresponding actin masks. ***$p < 0.001$. To see this figure in color, go online.

ICAM-1 nanoclusters. To further investigate and quantitate potential changes in ICAM-1 nanoscale organization as a result of shear flow, we used super-resolution STED microscopy, which is more amenable to apical membrane studies. With a spatial resolution of ∼90 nm, STED resolved individual ICAM-1 spots packed at different densities, both in static conditions and after 4 h of shear-flow stimulation (Fig. 4, *A–C*). The spot densities correlated well with the results shown in Fig. 1 *D*, i.e., more sparse spots were observed in the absence of shear flow (∼2 spots μm^{-2})

(Fig. 4 *A*) or in regions downstream of flow (∼1.2 spots μm^{-2}) (Fig. 4 *C*), whereas ICAM-1 spot density was much higher in regions of the membrane upstream of flow (∼4 spots μm^{-2}) (Fig. 4 *B*).

Aside from assessing the ICAM-1 spot density in the different conditions and EC regions, we also quantified the brightness (i.e., fluorescence intensity) of individual spots to inquire on the extent of ICAM-1 nanoclustering. As the intensity in each spot is proportional to the number of molecules inside a given spot, an increased spot intensity
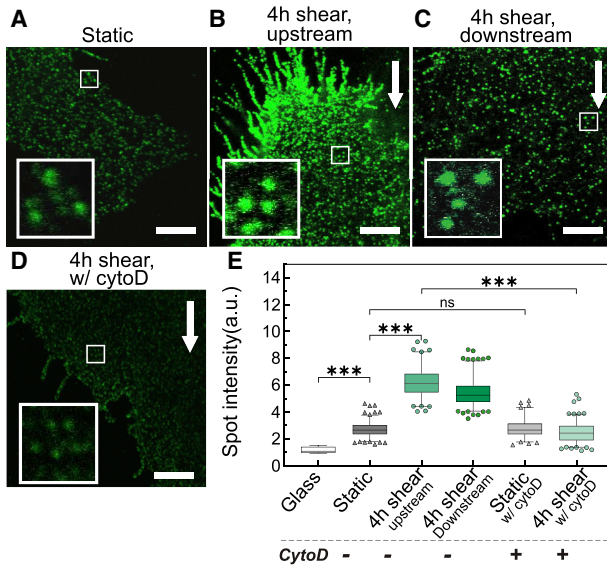
FIGURE 4 Shear flow promotes actin-dependent ICAM-1 nanocluster-ing on TNFα-treated ECs. Representative STED images of ICAM-1 taken in (*A*) static ECs; (*B*) after 4 h of shear-flow stimulation, upstream of flow; (*C*) after 4 h of shear-flow stimulation, downstream of flow; and (*D*) after 4 h shear-flow-stimulated ECs and 20 min of CytoD treatment, upstream of flow. White arrows indicate the flow direction. Scale bars, 4 μm. (*Insets*) Magnified views of ICAM-1 fluorescent spots (1.5 × 1.5 μm regions). (*E*) Normalized ICAM-1 spot intensity for different conditions, as extracted from the analysis of STED images. The intensity of ICAM-1 has been normalized to the mean intensity of individual Abs nonspecifically attached to the glass substrate (i.e., glass condition). Box and whiskers plots (*bars* show median values, quartile distribution in *boxes*; 2.5–97.5 percentile in *whiskers*, individual symbols are outliers) show spot intensity data for one representative experiment per condition on at least $n = 15$ cells per condition. Significance has been calculated within the experiment shown. N = 2 independent experiments per condition. ***$p < 0.001$; ns, not significant. To see this figure in color, go online.

compared with that of single antibodies on glass indicates the occurrence of multiple molecules in each spot, i.e., nanoclustering (38). We thus measured the fluorescence intensity of individual ICAM-1 spots over multiple STED images and compared it to that of sparsely scattered single fluorescence antibodies on the glass substrate. Under static conditions, the spots intensity showed on average a 2.7-fold increase in intensity as compared with individual fluorescence spots sparsely located on the glass coverslip (Fig. 4 *E*), in agreement with the dimeric structure of ICAM-1 (29). Remarkably, application of shear flow resulted in a sixfold increase in spot intensity, demonstrating the formation of ICAM-1 nanoclusters on the apical EC membrane both upstream and downstream of flow (Fig. 4 *E*).

To inquire whether the observed ICAM-1 nanoclustering depends on the actin cytoskeleton, we used a mild concentration of CytoD to disrupt the actin meshwork after shear-force stimulation and then imaged ICAM-1 distribution by STED. CytoD visibly perturbed the EC actin meshwork (Fig. S4 *A*) and caused marked changes in ICAM-1 nanoscale distribution (Fig. 4 *D*). Indeed, perturbation of

the actin cytoskeleton completely abrogated ICAM-1 nano-clustering with fluorescence spots having intensities comparable with those of static conditions (Fig. 4 *E*). Together, these results demonstrate that shear forces induce ICAM-1 nanoclustering before leukocyte engagement and underscore the crucial role of the actin cytoskeleton in forming and/or maintaining these nanoclusters. Of note, CytoD treatment did not affect ICAM-1 dimer distribution on static TNFα-treated ECs (Fig. 4 *E*), a result that is fully consistent with the notion that ICAM-1 is constitutively expressed as a dimer on the EC surface (29).

Changes in ICAM-1 spatial organization as a result of shear flow correlate with increased leukocyte migration across ECs

Upon inflammation, leukocytes migrate across the endothelium before extravasation in a process that is primarily mediated by interactions between ICAM-1 on the endothelium and its counterpart integrin receptor LFA-1 on the leukocyte membrane (2,7). To study the potential relevance of shear-flow-induced ICAM-1 gradient distribution and its nanoclustering on the arrest and migration of leukocytes, we performed two sets of parallel experiments (Fig. 5 *A*): one in which TNFα-treated ECs were first prestimulated for 4 h by shear flow and a second set of experiments in which the cells were not mechanically prestimulated (i.e., static). For both experimental conditions, we then flowed Jurkat T cells into the chamber, allowed them to settle on the ECs for 3 min, resumed the flow at 1 dyn cm^{-2} (postflow), and recorded T-cell movement for 20 min (Fig. 5 *A*).

Once subjected to postflow, 64% of T cells firmly adhered to ECs. These results were independent of whether ECs had been initially exposed to prolonged shear flow or not (Fig. 5 *B*), suggesting that the elevated expression levels of ICAM-1 on TNFα-treated ECs are sufficient to support cell adhesion. Adherent T cells on ECs underwent noticeable morphological changes in time. We mainly observed three different morphologies, which we classified as "round," "comet-like," and "amoeba-like," the latter being consistent with a promigratory phenotype (Fig. 5 *C*). A large majority (~70%) of T cells adhered to static ECs and in the absence of postflow remained round (Fig. 5 *D*, *black bars*), whereas 20 min of postflow stimulation on these static ECs showed no preference for a particular type of T-cell morphology (Fig. 5 *D*, *red bars*). In strong contrast, the majority of T cells (>60%) on shear-flow prestimulated ECs exhibited amoeba-like, promigratory morphology, regardless of whether the T cells had been additionally subjected to postflow or not (Fig. 5 *E*). These results indicate that prolonged prestimulation of ECs with shear flow promotes a more promigratory response of T cells.

In the case of shear-flow prestimulated ECs, around 90% of the T cells (total of 60) that showed migration had been initially adhered to EC regions upstream of flow (Fig. S5).
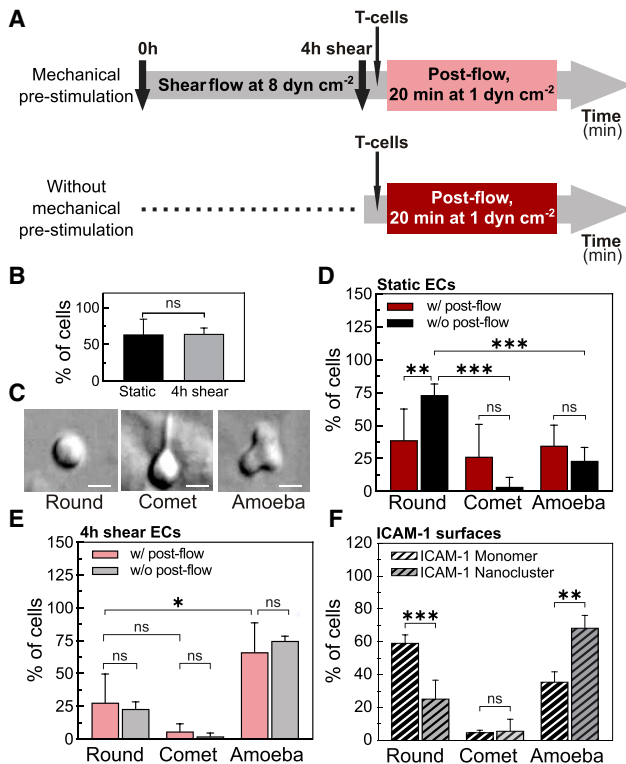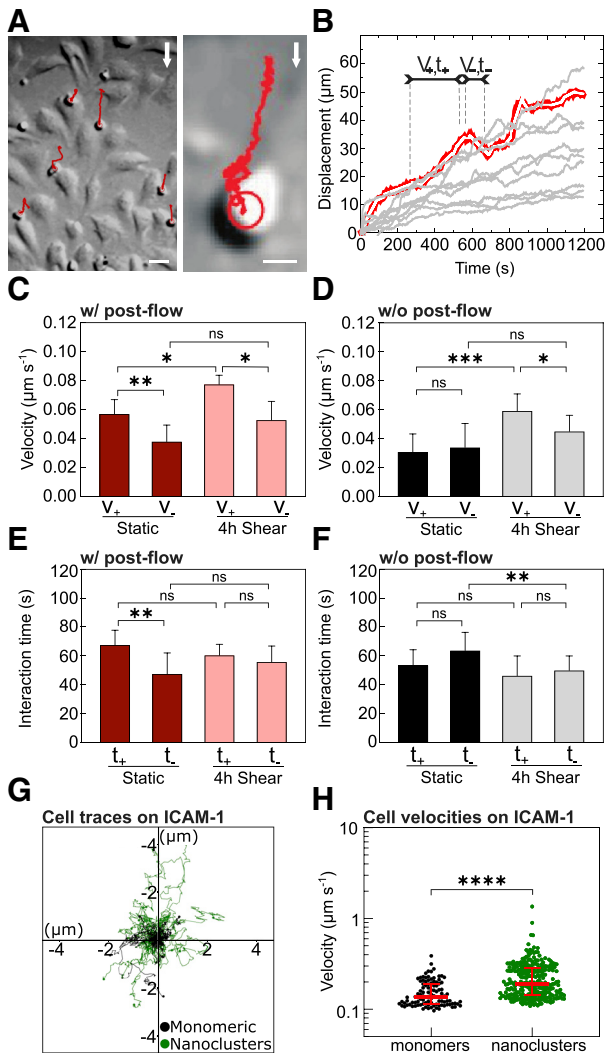
FIGURE 5 Prolonged shear stimulation of ECs promotes a promigratory phenotype in T cells. (*A*) Scheme showing the characteristic timescales and course of the experiments with (*top*) and without shear-flow prestimulation of ECs (*bottom*). (*B*) Percentage of T cells that remained adhered to ECs after 20 min of postflow application. Results are mean ± SD on N = 13 and N = 5 independent experiments for static and 4 h sheared ECs, respectively (at least $n = 10$ cells (static) and $n = 100$ cells (4 h shear) per experiment). Significance has been calculated across N. (*C*) DIC images showing the three main cell morphologies observed: "round," "comet-like," and "amoeba-like." Scale bars, 4 μm. (*D*) Percentage of T cells with indicated morphology adhered on static ECs (i.e., without mechanical prestimulation), with (w/, *red*) and without (w/o, *black*) postflow for 20 min. Results are mean ± SD on N = 6 and N = 4 independent experiments for w/ and w/o postflow, respectively (at least $n = 10$ T cells per experiment). Significance has been calculated across N. (*E*) Percentage of T cells with indicated morphology adhered to 4 h, shear-flow preconditioned ECs, with (w/, *light red*) and without (w/o, *gray*) postflow for 20 min. Results are mean ± SD on N = 5 and N = 4 independent experiments for w/ and w/o postflow, respectively (at least $n = 10$ T cells per experiment). Significance has been calculated across N. (*F*) Percentage of T cells with indicated morphology adhered to monomeric or nanoclustered ICAM-1-coated glass substrates. Results are mean ± SD on $n = 60$ cells (monomeric ICAM-1 substrates) and $n = 57$ cells (nanoclustered ICAM-1 substrates) for one representative experiment per condition. Significance has been calculated within the experiment shown. N = 3 independent experiments per condition ***$p < 0.001$; **$p = 0.01$; *$p = 0.1$; ns, not significant. To see this figure in color, go online.

Interestingly, these regions do coincide with those in which we had observed ICAM-1 enrichment and nanoclustering. On other EC regions, T cells did not stably adhere, and they were rapidly taken away by the flow. These observations suggest that ICAM-1 nanoclustering and its enrichment to regions upstream of flow might be responsible for the more promigratory phenotype of T cells. Unfortunately,

technical limitations associated with the labeling protocol for STORM and/or STED (i.e., requires cell fixation and Ab labeling) and its incompatibility with our current shear-flow system prevented us from directly correlating ICAM-1 distribution on ECs with T-cell attachment and/or migration. To overcome these limitations and to emulate the ICAM-1 shear-flow results, we assessed instead whether ICAM-1 distribution (monomer or nanoclustered) on glass-coated surfaces having the same overall ICAM-1 density would have an impact on T-cell phenotype. We induced ICAM-1 nanoclusters by means of polyclonal Abs against ICAM-1 (34), characterized them at the single-molecule level using low-density concentrations, and compared them to the signal from monomeric ICAM-1 to ensure the generation of small nanoclusters (Fig. S6, *A and B*). We then prepared fully coated ICAM-1 surfaces (monomeric versus nanoclustered) at equal coverage density (19 μg mL^{-1}) and seeded T cells on top. T cells adhered to these two types of substrates showed remarkable differences in their phenotype. Indeed, whereas on monomeric ICAM-1 surfaces most of the T cells remained round, ICAM-1 nanoclustered surfaces promoted a clear promigratory, amoeba-like morphology (Fig. 5 *F*). As additional controls, we seeded T cells on monomeric ICAM-1 surfaces at different densities, below and above 19 μg mL^{-1}. Whereas at low ICAM-1 concentrations, most cells did not bound to the surface, at concentrations of 19 μg mL^{-1} and 50 μg m^{-1} monomeric ICAM-1, cells bound but remained mostly round, without significantly increasing the fraction of amoeboid morphology (Fig. S6 *C*). Altogether, these results indicate that ICAM-1 nanoclustering is sufficient to induce changes on T-cell morphology toward a more promigratory profile.

To further investigate T-cell migration across ECs, we applied a tracking algorithm to reconstruct trajectories of individual T cells (37) as they migrate in the presence of postflow (Fig. 6 *A*). Individual T-cell trajectories were analyzed by using an additional algorithm that detected changes in the slopes of each trajectory and generated consecutive segments from which the instantaneous velocity (along or against the flow) of each segment and its time duration, i.e., interaction time, were extracted (37) (see Materials and methods) (Fig. 6 *B*). Cumulative frequency distributions of all the instantaneous velocities (positive when moving along the flow or negative when moving against the flow) and corresponding interaction times per experiment over multiple cells were generated, and the mean values per experiment were extracted.

T cells migrating across shear-flow prestimulated ECs and in the presence of postflow moved faster compared with their counterparts moving across static ECs (Fig. 6 *C*). The mean values of the instantaneous velocities along the direction of flow resulted $V_+ = (77 \pm 6)$ nm s^{-1} and $V_+ = (57 \pm 9)$ nm s^{-1} for shear-flow prestimulated and static ECs, respectively. Similar increase in T-cell velocities was also observed in the absence of postflow (Fig. 6 *D*),

FIGURE 6 Preconditioning of ECs by prolonged shear-flow stimulation influences T-cell migration. (*A*) Representative DIC (*left*) and zoom-in (*right*) images of T cells (*small round cells*) migrating in the presence of postflow over 4 h shear-flow prestimulated ECs (*large elongated cells*). Trajectories of T-cell movement are shown in red. White arrows indicate the flow direction. Scale bars, 20 μm (*left*) and 5 μm (*right*). (*B*) Characteristic time-trace plots (*gray curves*) of T-cell displacements in the direction parallel to the shear flow. The segmentation algorithm divides the curves into short line segments (*white segments* superimposed over the *red line*) from which positive and negative slopes, corresponding to the instantaneous T-cell velocity ($V_{+,-}$) and the time of interaction with ECs ($t_{+,-}$), are determined separately. (*C*) Mean instantaneous velocities of individual T cells subjected to postflow, migrating along (V_+) or against (V_-) the flow direction, over static and 4 h shear-flow-stimulated ECs. (*D*) Similar to (*C*) but without postflow. (*E* and *F*) Mean interaction times of individual T cells with ECs, with postflow (*E*) and without postflow (*F*). Results in (*C*) and (*E*) are mean $\pm$ SD on N $=$ 8 and N $=$ 4 independent experiments for static and 4 h shear, respectively (between $n = 5$ and 10 T cells per experiment). Significance has been calculated across N. Results in (*D*) and (*F*) are mean $\pm$ SD from two different experiments per condition, with $n = 10$ cells per experiment and condition. (*G*) Representative single-cell trajectories recorded on monomeric (*black*) or nanoclustered (*green*) ICAM-1 substrates. (*H*) Scatter plot of the instantaneous velocity of T cells migrating on the two types of substrates. Lines show the median and interquartile range from one representative experiment per condition (monomeric surfaces: $n = 103$ cell

indicating that the increased migration speed was due to the mechanical preconditioning of the ECs. These data are also consistent with the increased number of cells having a promigratory amoeba phenotype on prestimulated ECs (Fig. 5 *E*) and were, in fact, largely responsible for the increased velocities measured (Table S1).

In addition, the mean interaction time between T cells and ECs moving along the flow exhibited an opposite trend with respect to the velocity, being slightly shorter in the case of shear-flow prestimulated ECs as compared with static conditions and regardless of postflow, although these differences were not statistically significant among the different experiments (Fig. 6, *E and F*). When T cells migrated against the flow direction, their velocity was reduced, i.e., $V_- < V_+$, in particularly for T cells moving on prestimulated ECs (Fig. 6, *C and D*). In addition, the interaction time between T cells and ECs was in general somewhat shorter for T cells moving against the flow as compared with those ones moving along the flow ($t_- < t_+$), in particular under postflow conditions (Fig. 6, *E and F*). Altogether, these results indicate that although the directional motion of T cells on ECs is driven by the postflow, their migration behavior strongly depends on the preconditioning of ECs by shear flow stimulation; T cells migrating over mechanically prestimulated ECs move at higher speed and make shorter-lived contacts with ECs as compared with T cells migrating over static ECs.

Finally, to confirm that ICAM-1 nanoclustering induced by prolonged mechanical stimulation leads to increased T-cell migration speed, we resourced once more to ICAM-1-coated surfaces. We prepared coated surfaces with high-density monomeric or nanoclustered ICAM-1 and tracked the mobility of T cells (final concentration of $\sim$20 μg mL^{-1} of ICAM-1). Consistent with their increased promigratory phenotype on ICAM-1 nanoclustered substrates (Fig. 5 *F*), T cells migrated significantly faster on these substrates (Fig. 6, *G and H*), once more supporting the notion that ICAM-1 nanoclustering increases T-cell migration. As an additional control, we artificially induced ICAM-1 nanoclustering by antibody cross-linking of living TNFα-stimulated ECs and monitored T-cell migration. Also in these conditions, T cells migrated significantly faster as compared with control ECs (Fig. S7). Overall, our results strongly indicate that ICAM-1 nanoclustering brought about by shear flow increases T-cell migration.

DISCUSSION

In this work, we have used confocal and different forms of super-resolution microscopy, together with laminar flow, to assess the effect of shear forces on the lateral organization of

trajectories; nanoclustered surfaces: $n = 274$ cell trajectories). ****$p < 0.0001$; ***$p < 0.001$; **$p < 0.01$; *$p < 0.1$; ns, not significant. To see this figure in color, go online.

ICAM-1 on ECs and potential impact on leukocyte migration. Exposure of TNFα-stimulated ECs to shear flow promoted translocation of ICAM-1 to the upstream direction of flow, together with the formation of ICAM-1 nanoclusters on the EC membrane before leukocyte engagement. Moreover, shear-force-induced ICAM-1 nanoclustering is actin dependent. This shear-force-induced rearrangement of ICAM-1 and actin directly correlated with altered T-cell migration. Specifically, a more migratory phenotype, faster migration, and reduced interaction times of leukocytes with the opposing mechanically prestimulated EC surface were observed.

It has been extensively documented that shear flow induces major rearrangements of the actin cytoskeleton of ECs with the formation of rich actin fibers along the flow direction (19). Our super-resolution studies confirmed these changes and, importantly, also showed the formation of actin patches upstream of flow that localize to newly formed ICAM-1 nanoclusters. Formation of ICAM-1 nanoclusters was actin-cytoskeleton dependent, and disruption of the actin network led to the dissolution of the nanoclusters. Such local stability of ICAM-1 nanoclusters under shear flow might have been promoted by their anchoring to the actin cytoskeleton by means of different adaptor proteins, such as α-actinin-4 and cortactin (30). These actin-binding proteins can directly upregulate ICAM-1 clustering and, as such, enhance ICAM-1 adhesive function (27,30,39). It would be important to further identify which molecular actors are responsible for mechanosensing and the downstream signaling cascade that leads to actin remodeling and ICAM-1 nanocluster formation. Some initial work has been already done along these directions, showing that ICAM-1 itself is a force-sensing receptor (40), capable of initiating mechanosensitive signaling events such as recruitment of actin-binding proteins, increase of RhoA activity, and ROCK-myosin-based contractile forces (27). These rearrangements of the actin machinery could then feedback into ICAM-1, causing its spatial redistribution on the EC surface. Identifying the pathways involved into the mechanosensing and feedback amplification would provide a great opportunity to target specific steps in the process, which would strongly increase our understanding of the molecular mechanisms that underlie the described phenotypes.

Previous studies showed that artificially induced ICAM-1 clustering leads to its immobilization on the EC surface by binding of the ICAM-1 cytoplasmic tail to actin-binding proteins of the ERM and α-actinin families (18). More recently, actin-dependent clustering and ICAM-1 immobilization have been also observed upon dendritic cell maturation (31). Although, in our studies, we did not assess the mobility of the newly formed ICAM-1 nanoclusters, their dependence on the actin cytoskeleton and close proximity to actin patches suggest that these nanoclusters are also immobile. Immobilization of ICAM-1 has major consequences for immune responses that require firm adhesion. Indeed, interruption of ICAM-1 interactions with actinin

and members of the ERM family on ECs inhibits the ability of T cells to undergo diapedesis (39,41). Moreover, constrained ICAM-1 mobility on dendritic cells promotes T-cell conjugation during the immunological synapse, T-cell homotypic interactions, and T-cell proliferation (31). These processes are molecularly regulated by the ability of ICAM-1 to interact with its counterpart integrin receptor LFA-1. Integrin-dependent adhesion is regulated at two levels: affinity (the strength of each individual bond), which depends on the conformational state of the integrin and ability to bind its ligand, and valency (the total number of bonds). The product of affinity and valency provides the avidity and thus strength of the interaction between integrins and their ligands that enable adhesion (8). Immobilization and nanoclustering of ICAM-1 would impact both the affinity and valency of LFA-1. Whereas ICAM-1 immobilization could contribute to force-induced conformational changes that lead to LFA-1 activation (12,13), ICAM-1 nanoclustering would increase the number of interactions with LFA-1 molecules, thus augmenting avidity (10,11). Our work thus shows that application of shear forces impacts the spatiotemporal organization of ICAM-1 on ECs, directly affecting the regulatory mechanisms that govern integrin-mediated T-cell adhesion.

Our experiments further showed that T-cell migration depended on prolonged mechanical prestimulation of ECs. We observed a more migratory phenotype in T cells that adhered on mechanically stimulated ECs, and T-cell adhesion was significantly stronger on EC regions upstream of flow, where ICAM-1 levels were found to be the highest. Moreover, T cells moved faster with shorter interaction periods on ECs pre-exposed to mechanical stress. As ICAM-1 is one of the main ligand receptors implicated in the endothelium-leukocyte interaction by its engagement with LFA-1, we suggest that the changes in the migratory behavior of T cells should be, at least in part, associated to the spatiotemporal reorganization of ICAM-1 on the EC membrane brought about by shear flow. Indeed, control experiments on monomeric versus nanoclustered ICAM-1 surfaces conclusively showed that T cells adhered on these surfaces developed a promigratory profile and migrated faster as compared with monomeric ICAM-1 surfaces. We can qualitatively rationalize our results in the context of a recently proposed motor-clutch model (42). In essence, such a model predicts that cell velocity at the front edge is regulated by the tight interplay between the strength of engaged integrin-ligand bonds (i.e., clutches) and the stiffness of the substrate. Strengthening of the clutches will slow down actin retrograde flow (43), thus increasing the effective cell velocity at the front edge. In the context of our experimental results, an increase in ICAM-1 nanoclustering brought about by shear flow will increase the valency to LFA-1 molecules on the T-cell side, reinforcing clutching strength. In addition, as ICAM-1 nanoclusters could become immobilized by its interaction with the actin cytoskeleton (18,31), their engagement with LFA-1 will favor ligand-dependent integrin
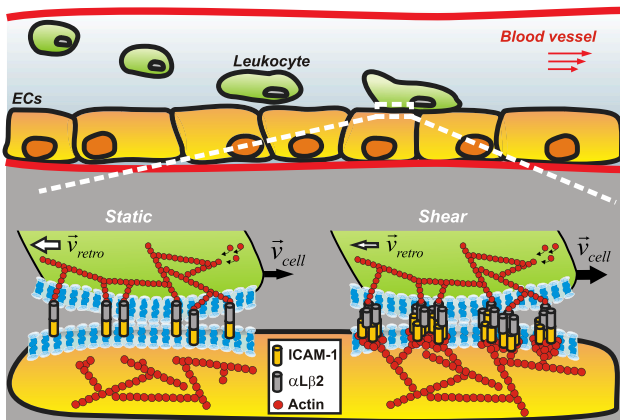
FIGURE 7 Shear flow promotes actin-dependent ICAM-1 nanocluster-ing on ECs that affect T-cell migration by strengthening interactions be-tween ICAM-1 and its integrin receptor LFA-1. Under static conditions, leukocyte engagement leads to the formation of bonds between individual ICAM-1 dimers and $\alpha L\beta 2$ (LFA-1) counter-integrin receptors. The strength of these bonds regulates leukocyte migration, with the total velocity of the cell edge (*black arrows*, V_{cell}) being determined by the difference between the speed of the actin-cytoskeleton polymerization and the speed of the actin retrograde flow (*white arrows*, V_{retro}). Shear-flow stimulation of ECs leads to actin-dependent ICAM-1 nanoclustering and most probably, its immobilization on the EC membrane. Both effects enhance the strength of ligand-integrin bonds by promoting integrin activation and increasing the avidity of ICAM-1 to LFA-1. This, in turn, reduces the retrograde actin flow rate and increases the total velocity of leukocytes as compared with static conditions. At the same time, as the cell moves forward, the immobilization of ICAM-1 nanoclusters will rapidly lead to ICAM-1-LFA-1 bond breakage, shortening the interaction times between the T cell and the EC, as compared with static conditions. The size of white and black arrows in-dicates the resulting velocity, with thicker arrows corresponding to higher speed values. To see this figure in color, go online.

activation (12,13), further contributing to increase integrin-ligand binding strength. This overall increase will result in a faster advance of T cells over the ECs, which fully agrees with our experimental observations.

According to the same model, stiffer substrates will induce the earlier break of the integrin-ligand bonds, with a consequent reduction of interaction times (42). In our ex-periments, we observed that ICAM-1 nanoclusters formed by shear stress localize to regions enriched with actin. Most probably, this limits their spatial diffusion and pro-motes immobilization (18,31) and effective stiffening on the regions of clutch anchoring. As the effective local sub-strate becomes stiffer, the bonds between fixed ICAM-1 and the actin-cytoskeleton-engaged integrins will break faster, reducing the time of interaction between T cells and ECs as observed in our experiments. The model pro-posed to connect our overall results is summarized in Fig. 7.

CONCLUSIONS

In summary, our results demonstrate for the first time, to our knowledge, that shear forces are sufficient to promote the formation of ligand receptor nanoclusters on the cell surface as a result of force-induced actin-cytoskeleton remodeling. Because many transmembrane receptors interact either directly or indirectly with the actin cytoskeleton, mechani-cal forces could represent an additional mechanism to orchestrate the lateral organization of a broad range of re-ceptors impacting in their function. In the context of this work, we show that the organization of ligand receptors on the EC membrane influences the migratory behavior of leukocytes. Such a physical mechanism might be of crucial importance for leukocyte-EC interactions during the immune response, in which the rapid and stable arrest of leukocytes on a vascular bed warrants their precise con-tact-mediated guidance. In this context, it would be impor-tant to assess the role of ICAM-1 polarization and clustering in vivo and its impact in leukocyte transendothelial migration.

SUPPORTING MATERIAL

AUTHOR CONTRIBUTIONS

ACKNOWLEDGMENTS

REFERENCES

1. Ley, K., C. Laudanna, …, S. Nourshargh. 2007. Getting to the site of inflammation: the leukocyte adhesion cascade updated. *Nat. Rev. Im-munol.* 7:678–689.

2. Nourshargh, S., and R. Alon. 2014. Leukocyte migration into inflamed tissues. *Immunity.* 41:694–707.

3. Imhof, B. A., and M. Aurrand-Lions. 2004. Adhesion mechanisms regulating the migration of monocytes. *Nat. Rev. Immunol.* 4:432–444.

4. Makgoba, M. W., M. E. Sanders, …, S. Shaw. 1988. ICAM-1 a ligand for LFA-1-dependent adhesion of B, T and myeloid cells. *Nature.* 331:86–88.

5. Marlin, S. D., and T. A. Springer. 1987. Purified intercellular adhesion molecule-1 (ICAM-1) is a ligand for lymphocyte function-associated antigen 1 (LFA-1). *Cell.* 51:813–819.

6. Abram, C. L., and C. A. Lowell. 2009. The ins and outs of leukocyte integrin signaling. *Annu. Rev. Immunol.* 27:339–362.

7. Hogg, N., I. Patzak, and F. Willenbrock. 2011. The insider's guide to leukocyte integrin signalling and function. *Nat. Rev. Immunol.* 11:416–426.

8. Kinashi, T. 2005. Intracellular signalling controlling integrin activation in lymphocytes. *Nat. Rev. Immunol.* 5:546–559.

9. Luo, B. H., C. V. Carman, and T. A. Springer. 2007. Structural basis of integrin regulation and signaling. *Annu. Rev. Immunol.* 25:619–647.

10. Bakker, G. J., C. Eich, …, M. F. Garcia-Parajo. 2012. Lateral mobility of individual integrin nanoclusters orchestrates the onset for leukocyte adhesion. *Proc. Natl. Acad. Sci. USA.* 109:4869–4874.

11. van Kooyk, Y., and C. G. Figdor. 2000. Avidity regulation of integrins: the driving force in leukocyte adhesion. *Curr. Opin. Cell Biol.* 12:542–547.

12. Nordenfelt, P., H. L. Elliott, and T. A. Springer. 2016. Coordinated integrin activation by actin-dependent force during T-cell migration. *Nat. Commun.* 7:13119.

13. Schürpf, T., and T. A. Springer. 2011. Regulation of integrin affinity on cell surfaces. *EMBO J.* 30:4712–4727.

14. Chen, W., J. Lou, and C. Zhu. 2010. Forcing switch from short- to intermediate- and long-lived states of the alphaA domain generates LFA-1/ICAM-1 catch bonds. *J. Biol. Chem.* 285:35967–35978.

15. Constantin, G., M. Majeed, …, C. Laudanna. 2000. Chemokines trigger immediate beta2 integrin affinity and mobility changes: differential regulation and roles in lymphocyte arrest under flow. *Immunity.* 13:759–769.

16. Li, N., H. Yang, …, M. Long. 2018. Ligand-specific binding forces of LFA-1 and Mac-1 in neutrophil adhesion and crawling. *Mol. Biol. Cell.* 29:408–418.

17. Shamri, R., V. Grabovsky, …, R. Alon. 2005. Lymphocyte arrest requires instantaneous induction of an extended LFA-1 conformation mediated by endothelium-bound chemokines. *Nat. Immunol.* 6:497–506.

18. van Buul, J. D., J. van Rijssel, …, P. L. Hordijk. 2010. Inside-out regulation of ICAM-1 dynamics in TNF-alpha-activated endothelium. *PLoS One.* 5:e11336.

19. Galbraith, C. G., R. Skalak, and S. Chien. 1998. Shear stress induces spatial reorganization of the endothelial cell cytoskeleton. *Cell Motil. Cytoskeleton.* 40:317–330.

20. Wojciak-Stothard, B., and A. J. Ridley. 2003. Shear stress-induced endothelial cell polarization is mediated by Rho and Rac but not Cdc42 or PI 3-kinases. *J. Cell Biol.* 161:429–439.

21. Davies, P. F., A. Robotewskyj, and M. L. Griem. 1994. Quantitative studies of endothelial cell adhesion. Directional remodeling of focal adhesion sites in response to flow forces. *J. Clin. Invest.* 93:2031–2038.

22. Butler, P. J., G. Norwich, …, S. Chien. 2001. Shear stress induces a time- and position-dependent increase in endothelial cell membrane fluidity. *Am. J. Physiol. Cell Physiol.* 280:C962–C969.

23. Yamamoto, K., and J. Ando. 2013. Endothelial cell and model membranes respond to shear stress by rapidly decreasing the order of their lipid phases. *J. Cell Sci.* 126:1227–1234.

24. Nakajima, H., and N. Mochizuki. 2017. Flow pattern-dependent endothelial cell responses through transcriptional regulation. *Cell Cycle.* 16:1893–1901.

25. Nagel, T., N. Resnick, …, M. A. Gimbrone, Jr. 1994. Shear stress selectively upregulates intercellular adhesion molecule-1 expression in cultured human vascular endothelial cells. *J. Clin. Invest.* 94:885–891.

26. Tsuboi, H., J. Ando, …, A. Kamiya. 1995. Flow stimulates ICAM-1 expression time and shear stress dependently in cultured human endothelial cells. *Biochem. Biophys. Res. Commun.* 206:988–996.

27. Schaefer, A., and P. L. Hordijk. 2015. Cell-stiffness-induced mechanosignaling - a key driver of leukocyte transendothelial migration. *J. Cell Sci.* 128:2221–2230.

28. Staunton, D. E., M. L. Dustin, …, T. A. Springer. 1990. The arrangement of the immunoglobulin-like domains of ICAM-1 and the binding sites for LFA-1 and rhinovirus. *Cell.* 61:243–254.

29. Yang, Y., C. D. Jun, …, J. H. Wang. 2004. Structural basis for dimerization of ICAM-1 on the cell surface. *Mol. Cell.* 14:269–276.

30. Schaefer, A., J. Te Riet, …, P. L. Hordijk. 2014. Actin-binding proteins differentially regulate endothelial cell stiffness, ICAM-1 function and neutrophil transmigration. *J. Cell Sci.* 127:4470–4482.

31. Comrie, W. A., S. Li, …, J. K. Burkhardt. 2015. The dendritic cell cytoskeleton promotes T cell adhesion and activation by constraining ICAM-1 mobility. *J. Cell Biol.* 208:457–473.

32. Noria, S., F. Xu, …, B. L. Langille. 2004. Assembly and reorientation of stress fibers drives morphological changes to endothelial cells exposed to shear stress. *Am. J. Pathol.* 164:1211–1223.

33. Ohta, S., S. Inasawa, and Y. Yamaguchi. 2015. Alignment of vascular endothelial cells as a collective response to shear flow. *J. Phys. D Appl. Phys.* 48:245401.

34. van Zanten, T. S., A. Cambi, …, M. F. Garcia-Parajo. 2009. Hotspots of GPI-anchored proteins and integrin nanoclusters function as nucleation sites for cell adhesion. *Proc. Natl. Acad. Sci. USA.* 106:18557–18562.

35. Millán, J., L. Hewlett, …, A. J. Ridley. 2006. Lymphocyte transcellular migration occurs through recruitment of endothelial ICAM-1 to caveola- and F-actin-rich domains. *Nat. Cell Biol.* 8:113–123.

36. Nelson, P. C., C. Zurla, …, D. Dunlap. 2011. Tethered particle motion as a diagnostic of DNA tether length. *Int. J. Nanomedicine.* 6:179–195.

37. Sosa-Costa, A., I. K. Piechocka, …, C. Manzo. 2018. PLANT: a method for detecting changes of slope in noisy trajectories. *Biophys. J.* 114:2044–2051.

38. van Zanten, T. S., J. Gómez, …, M. F. Garcia-Parajo. 2010. Direct mapping of nanoscale compositional connectivity on intact cell membranes. *Proc. Natl. Acad. Sci. USA.* 107:15437–15442.

39. Schnoor, M. 2015. Endothelial actin-binding proteins and actin dynamics in leukocyte transendothelial migration. *J. Immunol.* 194:3535–3541.

40. Liu, Z., N. J. Sniadecki, and C. S. Chen. 2010. Mechanical forces in endothelial cells during firm adhesion and early transmigration of human monocytes. *Cell. Mol. Bioeng.* 3:50–59.

41. Celli, L., J.-J. Ryckewaert, …, A. Duperray. 2006. Evidence of a functional role for interaction between ICAM-1 and nonmuscle alpha-actinins in leukocyte diapedesis. *J. Immunol.* 177:4113–4121.

42. Bangasser, B. L., G. A. Shamsan, …, D. J. Odde. 2017. Shifting the optimal stiffness for cell migration. *Nat. Commun.* 8:15313.

43. Thievessen, I., P. M. Thompson, …, C. M. Waterman. 2013. Vinculin-actin interaction couples actin retrograde flow to focal adhesions, but is dispensable for focal adhesion growth. *J. Cell Biol.* 202:163–177.